




Synthesis of Fe₃O₄ Nanoparticles with Different Shapes Through a Co-Precipitation Method and Their Application

MUNEER M. BA-ABBAD ^{1,3} ABDELBAKI BENAMOUR,¹
DINA EWIS,¹ ABDUL WAHAB MOHAMMAD,²
and EBRAHIM MAHMOUDI²

1.—Gas Processing Centre, College of Engineering, Qatar University, P.O.Box 2713, Doha, Qatar.
2.—Department of Chemical and Process Engineering, Faculty of Engineering and Built Environment, Universiti Kebangsaan Malaysia, 43600 Bangi, Selangor Darul Ehsan, Malaysia.
3.—e-mail: mbaabbad@qu.edu.qa

Magnetic Fe₃O₄ nanoparticles (NPs) were successfully synthesized via co-precipitation method using ferric chloride and ferrous sulphate as the starting materials. The shape and the size of Fe₃O₄ NPs were controlled by using different types of additive including ammonium hydroxide and sodium hydroxide. The results revealed that by adding ammonium hydroxide, the particles attained a spherical shape with a uniform size. On the other hand, the shape of the particles turned from spherical to cubic using sodium hydroxide. The magnetic results showed that both samples attained hysteresis loop, which indicated that both samples have ferromagnetic behavior. In addition, Fe₃O₄ NPs with cubic shape showed higher adsorptive behaviour towards Congo red compared to spherical Fe₃O₄ NPs, which is attributed to the enhancement of their magnetic properties. The adsorption of Congo red onto cubic Fe₃O₄ NPs was best described by Langmuir isotherm model, while spherical Fe₃O₄ NPs followed Freundlich isotherm model.

INTRODUCTION

In the last 2 decades, nanomaterials especially metal oxides, have been used extensively as a magnetic storage material and catalyst because of their good mechanical and magnetic properties.¹ Iron oxide nanoparticles (Fe₃O₄ NPs) are the most famous and popular kind of magnetite nanomaterials and are used extensively in many applications because of their low cost, low toxicity and good magnetic properties.² Generally, the physical and chemical properties of magnetic nanomaterials depend on their morphology (shape) and size.³ These magnetic nanomaterials are mainly prepared in the presence of two major aqueous solutions, which are ferrous and ferric, using different methods such as co-precipitation, micro-emulsion technique and hydrothermal synthesis.^{4–6} Magnetic Fe₃O₄ NPs have been synthesized with different morphologies such as nanoparticles, nanocubes,

octahedral and rhombic dodecahedrons.⁷ Controlling the morphology and size of Fe₃O₄ NPs by controlling the reaction conditions has been reported previously.^{8,9} Recently, considerable efforts have been made to produce particles with interesting properties that can be used for wide range of applications. Most of the studies reported in the literature focused on controlling the spherical shape and the properties of Fe₃O₄ NPs, and few focused on producing cubic Fe₃O₄ NPs.^{10,11} Therefore, in this study, Fe₃O₄ nanoparticle shape was successfully controlled by different types of additive ammonia (NH₃) and sodium hydroxide (NaOH) in a conventional co-precipitation method. The solution pH and ratio between Fe⁺²/Fe⁺³ as well as the temperature of reaction were controlled to produce cubic Fe₃O₄ NPs with enhanced properties compared to spherical Fe₃O₄ NPs.

EXPERIMENTAL

Materials

To synthesize Fe_3O_4 NPs with different sizes and shapes, ferric chloride hexahydrate ($\text{FeCl}_3 \cdot 6\text{H}_2\text{O}$) and ferrous sulphate heptahydrate ($\text{FeSO}_4 \cdot 7\text{H}_2\text{O}$) were used (supplied by Merck, Germany, and Bendosen companies, respectively). Ammonium hydroxide (NH_4OH , with 30% of ammonia in water) and sodium hydroxide (NaOH , with concentration of 1 N = 1 mol/l) were obtained from R&M Chemicals, Malaysia, and Merck, Germany, respectively. Ethanol ($\text{C}_2\text{H}_5\text{OH}$), which is the solvent used as reaction medium, was purchased from R&M Chemicals. The Congo red dye was provided by R&M Chemicals Company.

Fe_3O_4 NPs Preparation

The co-precipitation method was applied to synthesize and control Fe_3O_4 NPs shape and size. Briefly, $\text{FeSO}_4 \cdot 7\text{H}_2\text{O}$ and $\text{FeCl}_3 \cdot 6\text{H}_2\text{O}$ were dissolved separately in two 50-ml beakers of water (A) and ethanol (B) under continuous stirring at room temperature. The molar ratio of $\text{FeSO}_4 \cdot 7\text{H}_2\text{O}$ and $\text{FeCl}_3 \cdot 6\text{H}_2\text{O}$ as Fe^{2+} and Fe^{3+} was 2 to 1 moles, respectively. After both solutions were completely dissolved, solution from beaker A was added slowly to beaker B, and the temperature was increased to $35 \pm 5^\circ\text{C}$. The final solution pH was adjusted by adding NH_4OH to reach pH 11.0 (Sample 1). The first procedure was repeated by changing the additive to NaOH to adjust the pH at 11.00 (Sample 2). Both samples were stirred vigorously at $60 \pm 5^\circ\text{C}$ for 2 h. After 2 h, the samples were left to cool down. Then, both samples were washed to remove unreacted precursors. The washing step was carried out with pure water continuously until the solution pH reached 7.0 ± 0.2 . Finally, both samples were washed by absolute ethanol and dried in an oven for 24 h at 75°C .

Characterization of Fe_3O_4 NPs

The structural phase and crystal size of the synthesized Fe_3O_4 NPs were evaluated using x-ray diffraction analysis. This analysis was carried out using the BRUKER AXS D8 ADVANCE diffraction meter (Bruker AXS, GmbH) with $\text{CuK}\alpha$ radiation ($\lambda = 1.5406\text{\AA}$) with scanning in range of $5\text{--}80^\circ$ for 2θ angle. The crystal size, d , of synthesized samples was calculated using the Scherrer equation (Eq. 1):

$$d = \frac{K\lambda}{\beta \cos \theta} \quad (1)$$

where K is the Scherrer constant, ($K = 0.89$), β is the peak width at half maximum (radian), λ is the x-ray wavelength, ($\lambda = 1.5406\text{\AA}$), and θ is the Bragg diffraction angle. To determine sizes and shapes of Fe_3O_4 NPs samples, a transmission electron microscope (TEM) (Philips CM200, model JEOLJEM

2100) and field emission scanning electron microscope (FESEM) (SUPRA 55VP) were used, respectively. Energy-dispersive x-ray spectroscopy (EDX) (Oxford EDX INCA Penta FETX3) was also used to measure composition of Fe_3O_4 samples.

The magnetic properties were investigated at room temperature using a vibrating sample magnetometer (VSM model Lakeshore 7404). The x-ray photoelectron spectroscopy (XPS) (Axis Ultra DLD, KRATOS model) was used to detect energy binding and oxidation state of Fe_3O_4 samples. This analysis was carried out with a monochromated Al $\text{K}\alpha$ (1486.6 eV) radiation as excitation source at 15 kV.

Experimental Procedures for Adsorption Process

The performance of both Fe_3O_4 NPs for the removal of Congo red dyes from aqueous solution was investigated in a batch process at room temperature; 50 mL of Congo red solution with selected loading of Fe_3O_4 NPs was shaken using a shaker. The initial concentrations of Congo red dyes ranged from 12.50 mg/L to 100 mg/L, and the loading of both Fe_3O_4 NPs ranged from 0.25 g/L to 2.0 g/L. After 30 min of shaking the samples, the mixture was centrifuged at 8000 rpm for 5 min. The removal ($R\%$) was measured using the absorption band in UV spectrum at wavelength of $\lambda_{\text{max}} = 500$ nm. The Congo red concentration for standard and residual was calculated from absorbance measured by Perkin Elmer (lambda 35) UV/Vis spectrophotometer. The efficiency of Congo red removal percentage was calculated from Eq. 2:

$$\text{Removal } (R\%) = \frac{C_0 - C_f}{C_0} \times 100 \quad (2)$$

where C_0 is the initial concentration and C_f the final concentration of Congo red dye, which were measured from the absorbance before and after adsorption process.

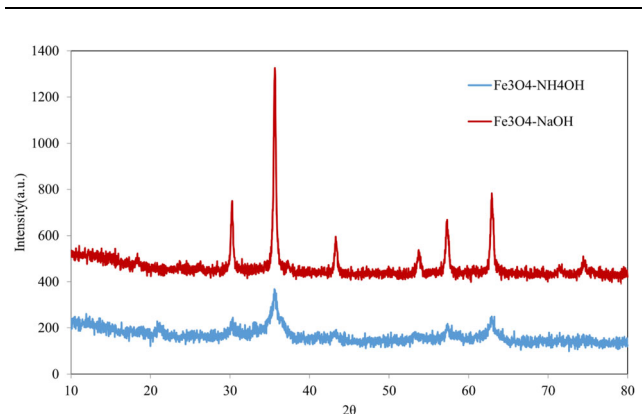


Fig. 1. XRD pattern of Fe_3O_4 NPs using different additives of NH_4OH and NaOH .

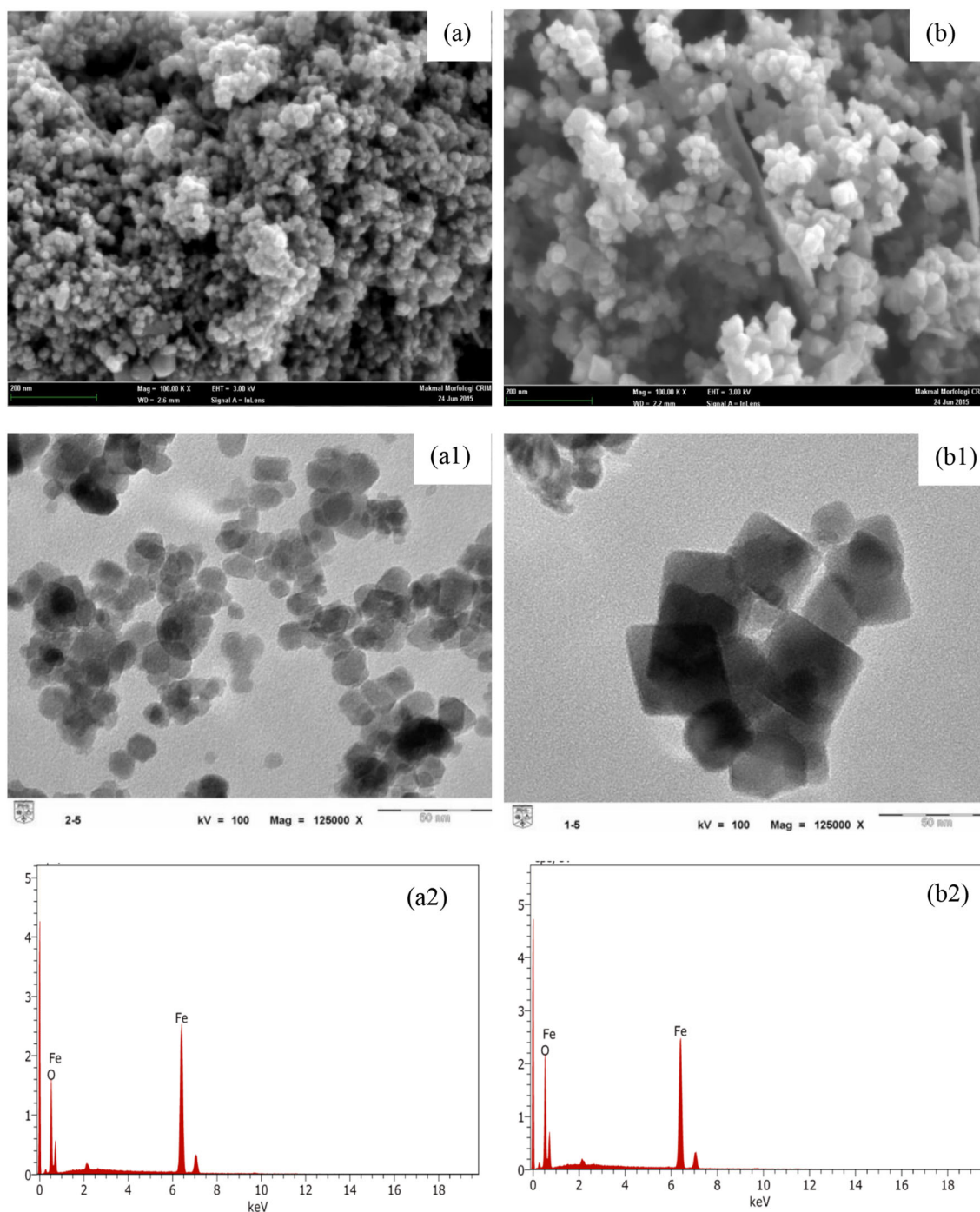


Fig. 2. FESEM, TEM images and EDX of Fe₃O₄ NPs synthesized using Fe₃O₄- NH₄OH (a, a1, a2) and Fe₃O₄- NaOH (b,b1,b2).

RESULTS AND DISCUSSION

XRD Analysis

The XRD patterns of Fe₃O₄ NPs prepared by co-precipitation method using different additives of NH₄OH and NaOH are shown in Fig. 1. The XRD diffraction peaks of both samples indicate a cubic system Fd-3m space group as phase structure, which in a good agreement with the standard (standard reference as ICDD: 98-015-8743).

However, all peak positions of Fe₃O₄ matched at 2θ of 30.21°, 35.72°, 43.34°, 53.35°, 57.37°, and 63.07°. The locations of the diffraction peaks were referred to the diffraction data of face-centered cubic (FCC) crystalline structure as reported earlier.¹² Lower intensity peaks of Fe₃O₄- NH₄OH compared to Fe₃O₄- NaOH were obtained, which was attributed to smaller crystal size of Fe₃O₄-NH₄OH compared to Fe₃O₄- NaOH. According to Scherrer Eq. (1), the average crystallite sizes were

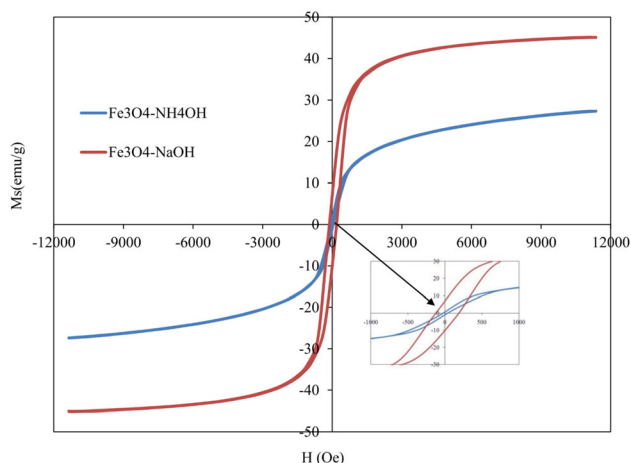


Fig. 3. Hysteresis loop of synthesized samples of both $\text{Fe}_3\text{O}_4\text{-NH}_4\text{OH}$ (spherical) and $\text{Fe}_3\text{O}_4\text{-NaOH}$ (cubic).

found to be 8 nm and 25 nm for Fe_3O_4 NPs using NH_4OH and NaOH , respectively. This result was also confirmed by the TEM analysis of both samples, which was in good agreement with the XRD values.

Surface Morphology

The size and the shape of the synthesized Fe_3O_4 NPs by both NH_4OH and NaOH are characterized using FESEM/EDX and TEM, as given in Fig. 2. The results of FESEM and TEM images indicated that Fe_3O_4 NPs attained a spherical shape using NH_4OH , while cubic shape was observed when using NaOH . The TEM images of both samples showed clearly that the Fe_3O_4 NPs shape was affected significantly by the type of additive, either NH_4OH or NaOH . Furthermore, the average sizes of the samples were evaluated as 10 ± 2 nm for $\text{Fe}_3\text{O}_4\text{-NH}_4\text{OH}$ and 32 ± 2 nm for $\text{Fe}_3\text{O}_4\text{-NaOH}$. By comparing the particle size of both samples, the TEM images showed that the particles size was larger than the values obtained from XRD. This was mainly because the TEM technique determines the diameter from the surface of the particle, while the XRD measures the single crystal grain.¹³ The energy-dispersive x-ray spectroscopy (EDX) results of both samples $\text{Fe}_3\text{O}_4\text{-NH}_4\text{OH}$ and $\text{Fe}_3\text{O}_4\text{-NaOH}$ are shown in Fig. 2. Only two peaks appeared in the spectrum for the oxygen (O) and iron (Fe), and their value of Fe was 78.14% and O was 21.86% for $\text{Fe}_3\text{O}_4\text{-NH}_4\text{OH}$; Fe was 76.54% and O was 23.46% for $\text{Fe}_3\text{O}_4\text{-NaOH}$. This result demonstrated that pure Fe_3O_4 was produced using NH_4OH and NaOH .¹⁴

Magnetic Properties

The magnetic properties of synthesized Fe_3O_4 NPs using different types of additives were measured at room temperature. Figure 3 shows the typical magnetic hysteresis loop of Fe_3O_4 NPs with spherical and cubic shape obtained with different

types of additives. The magnetic results of both samples showed a hysteresis loop, which indicated a ferromagnetic behavior. The ferromagnetic behavior of $\text{Fe}_3\text{O}_4\text{-NH}_4\text{OH}$ (spherical) showed saturation magnetization (Ms) and coercivity (Hc) values of 27.35 emu/g and 32.09 Oe, respectively. However, higher saturation magnetization (Ms) of 45.14 emu/g and coercivity (Hc) values and 129.73 Oe was obtained for $\text{Fe}_3\text{O}_4\text{-NaOH}$ (cubic). The results of magnetic properties show that saturation magnetization and value coercivity were enhanced when the shape of Fe_3O_4 NPs changed from spherical to cubic. These results were attributed to the large sharp anisotropic nature of the cubic, which represented the barrier for particle remagnetization.^{15,16}

XPS Analysis

Figure 4 shows the XPS spectra analysis for $\text{Fe}_3\text{O}_4\text{-NH}_4\text{OH}$ and $\text{Fe}_3\text{O}_4\text{-NaOH}$. The XPS spectra had a high detecting potential of Fe^{2+} and Fe^{3+} cations in Fe_3O_4 samples. However, herein, XPS was applied to determine the electronic properties and the chemical state information of the synthesized Fe_3O_4 NPs. Figure 4a and a1 shows the XPS analysis of the synthesized $\text{Fe}_3\text{O}_4\text{-NH}_4\text{OH}$, which indicates the detection of Fe 2p region as Fe 2p_{1/2} and Fe 2p_{3/2} at 723.50 and 711.30 eV, respectively. The XPS analysis of $\text{Fe}_3\text{O}_4\text{-NaOH}$ showed that no differences were obtained compared to $\text{Fe}_3\text{O}_4\text{-NH}_4\text{OH}$ in which 723.80 eV and 710.70 eV for Fe 2p_{1/2} and Fe 2p_{3/2}, respectively, as shown in Fig. 4b and b1. Oxygen (O 1s) was detected at region of 530.50 eV for both samples. These binding energies of Fe 2p_{1/2} and Fe 2p_{3/2} were in good agreement with the bulk Fe_3O_4 NPs binding energies.¹⁷ The XPS spectra showed that there were no other peaks for other magnetic compounds such as Fe_2O_3 , FeO and FeOOH. Generally, the higher binding energy of the Fe^{3+} compared to Fe^{2+} is attributed to an increased positive charge. Therefore, the overall shielding of the Fe^{3+} nucleus decreased, causing the electrons to be pulled closer to the Fermi level.^{18,19}

Mechanism of Shape Transformation

In general, control of nanoparticle morphology has been reported as the main challenge for researchers because several variables must be controlled within formation of the nanoparticles. In this study, we aimed to produce Fe_3O_4 and develop its properties and morphology using a common method. For this aim, the different precursor salts [ferric chloride hexahydrate ($\text{FeCl}_3 \cdot 6\text{H}_2\text{O}$) and ferrous sulphate heptahydrate ($\text{FeSO}_4 \cdot 7\text{H}_2\text{O}$)] and solvents, ammonia (NH_3) and sodium hydroxide (NaOH), were used and modified to tune Fe_3O_4 NPs shape controlling by the reaction temperature. This factor directly affected the kinetics of the reaction and the nucleation rate of the nanoparticles.²⁰ The main reaction to produce Fe_3O_4 NPs using Fe^{2+} and Fe^{3+}

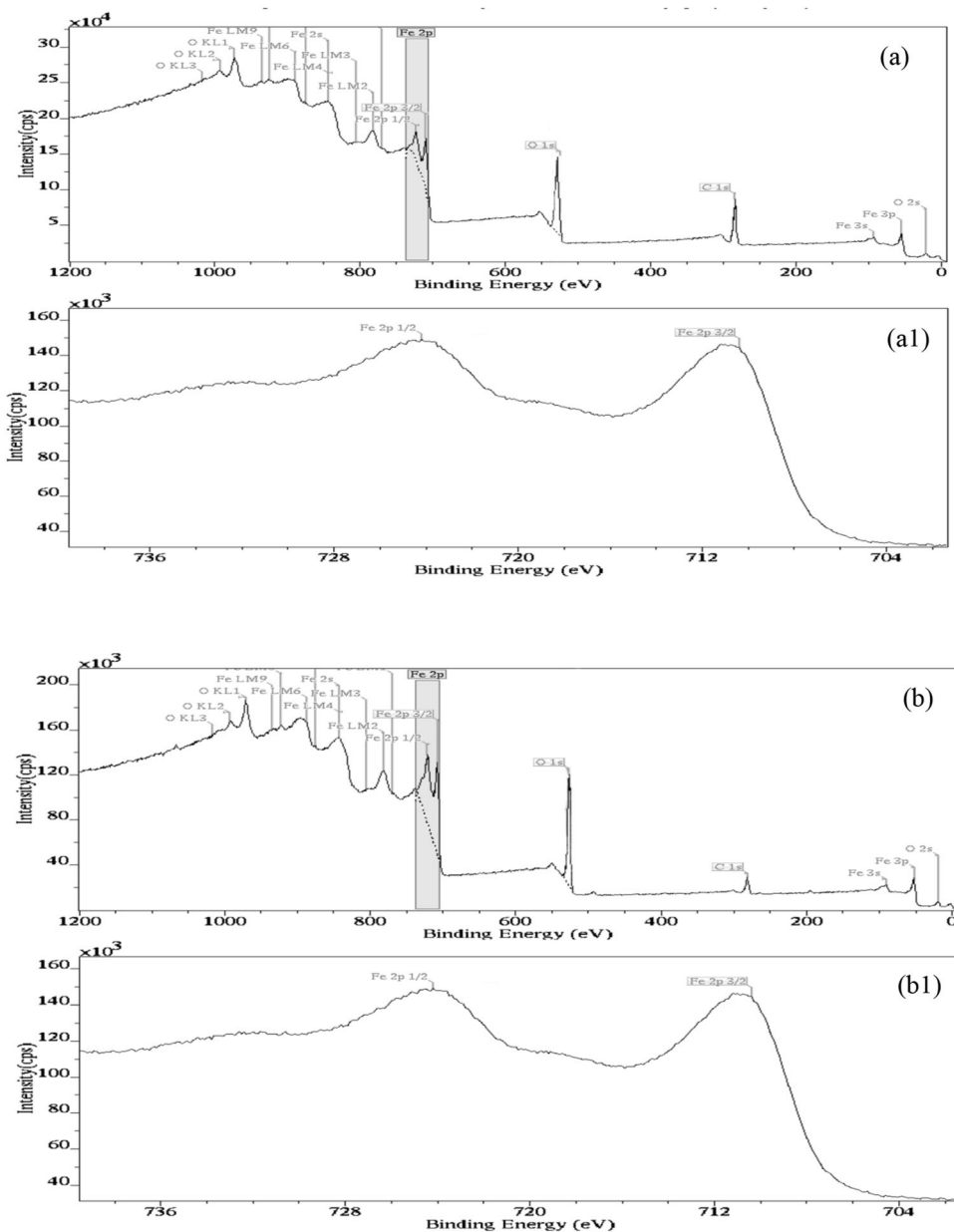
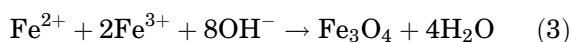
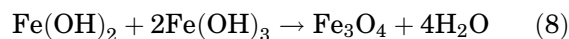
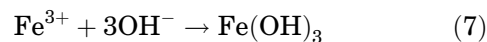
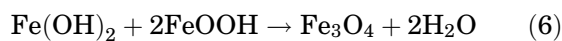
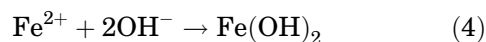


Fig. 4. XPS spectra of synthesized sample (a, a1) Fe₃O₄- NH₄OH (spherical) and (b, b1) Fe₃O₄- NaOH (cubic).

cations and NH₄OH, NaOH is given in the following Eq. 3:



On the other hand, some sequence reactions controlling Fe₃O₄ NPs morphology and properties, as reported in previous studies,²¹ are summarized in Eqs. 4, 5, 6, 7, and 8:



The mechanism of Fe₃O₄ NP formation with different morphologies (shapes) depended on the addition of NH₄OH and NaOH. By adding NH₄OH solution, the pH was slowly increased until it reached to 11.00, whereby a low concentration of

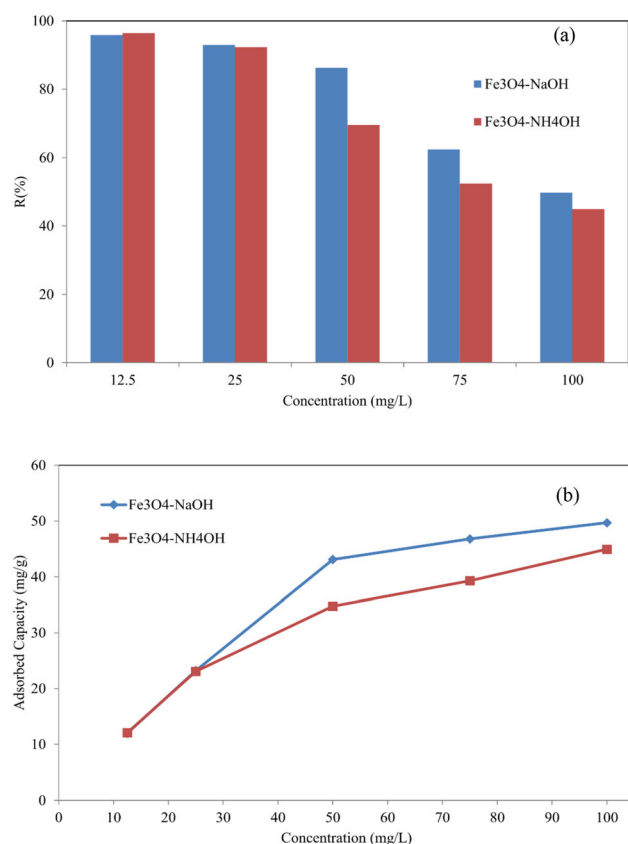


Fig. 5. Effects of initial concentration on: (a) removal efficiency, (b) adsorption capacity, (loading Fe₃O₄ NPs of 1g/l, pH = 7.0).

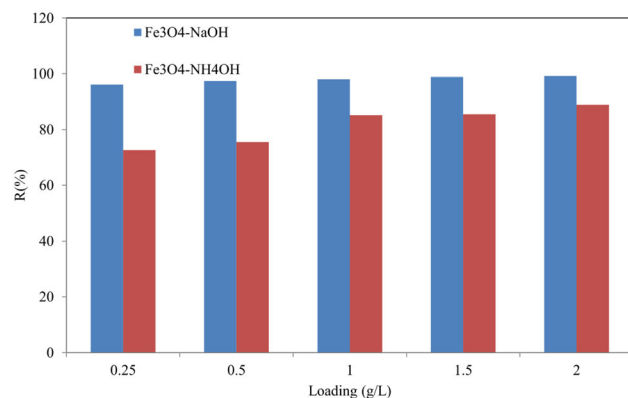


Fig. 6. Effects of the Fe₃O₄ NPs loading on the removal of Congo red dyes with concentration of 25 mg/L.

Fe(OH)₂ and FeOOH led to slow formation of Fe₃O₄ NPs (Eq. 6) with smaller particle size.²¹ However, by using NaOH solution, it caused the pH to reach 11 quickly, and the excess amount of OH⁻ led to an increase of Fe(OH)₂ and FeOOH concentrations (Eqs. 5 and 6). This condition showed faster growth of Fe₃O₄ NPs with large particle size.^{21,22} Actually, Fe₃O₄ NPs has a cubic crystal structure (FCC) whereby the surface energy is of anisotropic order as [111] < [100], which indicates that Fe₃O₄ crystal might have a tendency to grow in octahedral

structure.²⁰ However, changes of growth rate between the [111] and [100] facets resulted in one of them having lower surface energy than the other facet, which caused the change in structure morphology.²³ Furthermore, increase of reaction temperature led to destabilizing of [111] and [111] > [100], which allowed transforming the morphology to cubic shape.²³

Removal of Congo Red From Aqueous Solution

Figure 5 shows the removal efficiency (R%) and adsorption capacity of Congo red using Fe₃O₄-NH₄OH and Fe₃O₄-NaOH NPs at room temperature. However, the initial concentration of Congo red is one of the important factors that can affect the particles' adsorption efficiency. It is important to investigate the effect of initial pollutant concentration as it affects the adsorption capacity of the adsorbate because of the change in driving force strength between molecules in aqueous and solid phases.²⁴ The removal of Congo red exhibited was high under concentration < 50 mg/l for both samples, as shown in Fig. 5a. However, removal efficiency (R%) was reduced when the initial concentration was increased to > 50 mg/L for both samples. At the same time, higher removal was achieved by Fe₃O₄-NaOH compared to Fe₃O₄-NH₄OH for concentrations between 50 mg/L and 100 mg/L. On the other hand, an increase in the adsorption capacity with increasing Congo red concentration was observed by Fe₃O₄-NaOH, as shown in Fig. 5b. In addition, the adsorption equilibrium increased from 12 mg/g to 50 mg/g for Fe₃O₄-NaOH and from 12 mg/g to 44 mg/g for Fe₃O₄-NH₄OH. Overall, these results confirmed strong chemical interactions between the magnetic NPs and Congo red molecules [25]. It was postulated that the shape and higher magnetic properties of Fe₃O₄-NaOH not only caused the higher removal efficiency but also enhanced the capacity of adsorption.²⁵

The effect of loading on the Congo red removal at concentration of 25 mg/L was evaluated for both samples (Fig. 6). High removal using Fe₃O₄-NaOH was achieved for all loading compared to Fe₃O₄-NH₄OH. For the Fe₃O₄-NH₄OH sample, the removal efficiency increased from 72% to 88% as the NPs concentration increased from 0.25 g/L to 1 g/L. However, there was a slight increase (around 4%) in the removal efficiency of Congo red as the loading increased from 1.5 g/L to 2 g/L. These results indicated that the optimum dosage was around 0.25 g/L and 2 g/L from Fe₃O₄-NaOH and Fe₃O₄-NH₄OH, respectively. Overall, Fe₃O₄-NaOH samples showed higher removal capability at higher Congo red concentration because of their enhanced magnetic properties. However, electrostatic attraction between the Congo red molecules might be enhancing the adsorption mechanism.²⁶⁻³⁰

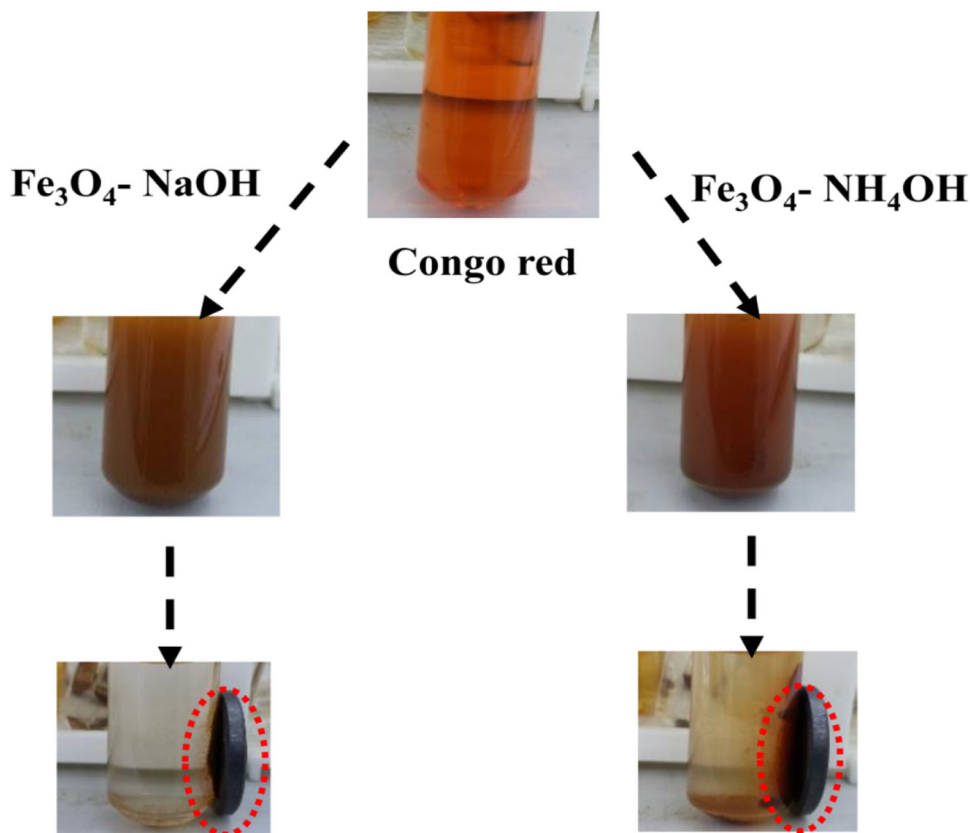


Fig. 7. Photo illustration of the performance of Fe₃O₄ NPs samples for Congo red removal and their recovery.

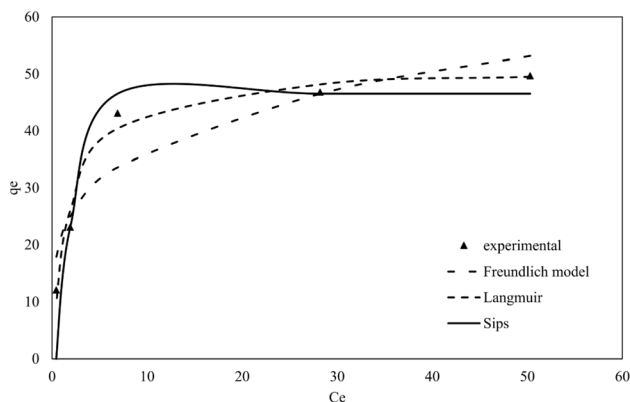


Fig. 8. Non-linear isotherm model fitting for Fe₃O₄-NaOH.

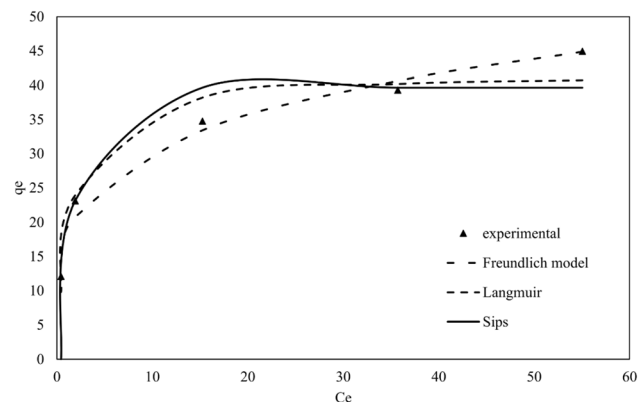


Fig. 9. Non-linear isotherm model fitting for Fe₃O₄-NH₄OH.

To investigate both Fe₃O₄ NPs samples' performance for Congo red removal, photos during adsorption experiments were taken as presented in Fig. 7. After shaking the Fe₃O₄ NPs samples with Congo red solution for 30 min, the NPs were collected using small pieces of magnetic. The results showed that the separation of Fe₃O₄- NaOH NPs was easy, and the solution become clear in few seconds. However, Fe₃O₄- NH₄OH NP separation using a magnet was slow, which could be attributed

to its weak magnetic property compared to Fe₃O₄-NaOH, as given and explained in Fig. 3. These results also confirm that good magnetic properties of both Fe₃O₄ NPs reduce the post-treatment time, which could affect the total cost in the future.

Adsorption isotherm

The adsorption data were fitted to the adsorption isotherm models to gain insights into the interaction between the adsorbents and Congo red, indicating a

Table I. Isotherm parameters for Langmuir, Freundlich and Sips models

Model	Parameter	Fe ₃ O ₄ -NaOH	Fe ₃ O ₄ -NH ₄ OH
Langmuir	K_L (L/mg)	0.535	0.695
	q_m (mg/g)	51.34	41.80
	R^2	0.979	0.948
	RMSE	2.143	2.690
Freundlich	K_F	21.51	17.87
	n_F	4.33	4.35
	R^2	0.872	0.976
	RMSE	5.270	1.816
Sips(L-F)	q_m (mg/g)	46.53	39.65
	b (L/mg)	0.00150	0.00147
	n	0.101	0.0952
	R^2	0.846	0.818
	RMSE	5.785	6.276

chemical or physical based adsorption process.³¹ In addition, the parameters obtained from adsorption isotherm models are important in designing adsorption contactors.³²

The equilibrium data were fitted to Langmuir, Freundlich and Sips isotherm models using nonlinear regression by employing Marquardt-Levenberg algorithm. Langmuir isotherm model assumes a monolayer adsorption over a homogenous surface that has identical surface energy. The model is described by Eq. 9.

$$Q_e = \frac{q_m K_L C_e}{(1 + K_L C_e)} \quad (9)$$

where K_L is the Langmuir constant in L/mg and q_m is the maximum adsorption capacity in mg/g.

Freundlich model assumes the adsorption occurs on a heterogeneous surface in which multilayer of adsorption occurs. The model is expressed by Eq. 10.

$$Q_e = K_f \cdot C_e^{1/n} \quad (10)$$

where n is the adsorption efficiency and K_f ($L^n \text{ mg}^{-1/n}/\text{g}$) is related to the adsorption capacity.

Sips model is a combination of Langmuir and Freundlich model, eliminating the restriction of limited adsorbate concentration range by Freundlich model. The model predicts a heterogeneous adsorption indicated by Freundlich model at low concentration range, while a monolayer adsorption is indicated by Langmuir model at higher concentration. The model is described by Eq. 11.

$$Q_e = \frac{q_m b C_e^{1/n}}{1 + b C_e^{1/n}} \quad (11)$$

where q_m is the maximum adsorption capacity in mg/g, b is related to energy of adsorption in L/mg, and n is sips isotherm constants.

The fitting of Congo red adsorption onto Fe₃O₄-NaOH and Fe₃O₄-NH₄OH is shown in Figs. 8 and 9, respectively. The associated parameters obtained

from the indicated models are shown in Table I. From Table I, the results clearly indicate that the adsorption of Congo red onto Fe₃O₄-NaOH followed the Langmuir model with coefficient of determination (R^2) value of 0.979 and root mean square error (RMSE) of 2.143 with a maximum adsorption capacity of 52.34 mg/g, while Congo red adsorption onto Fe₃O₄-NH₄OH was best fitted to Freundlich isotherm mode with R^2 value of 0.976 and RMSE value of 1.816. The cubic shape that Fe₃O₄-NaOH NPs attained facilitated monolayer adsorption of Congo red and eliminated the possibility of multilayer adsorption. On the other hand, the adsorption of Congo red onto Fe₃O₄-NH₄OH NPs was best explained by Freundlich isotherm model indicating a multilayer adsorption on a heterogeneous surface, which was mainly facilitated by the spherical shape that Fe₃O₄-NH₄OH NPs attained.

CONCLUSION

Controlling the shape and size of Fe₃O₄ NPs was successfully achieved by co-precipitation method using two different additives as reactants. The results showed that the additive type was the key to control shape and size of Fe₃O₄ NPs. The higher crystallized single cubic and spherical shapes of Fe₃O₄ were produced in the presence of sodium hydroxide and ammonia. The ferromagnetic properties at room temperature of the cubic showed higher saturation magnetization (Ms) and coercivity (Hc) values compared with spherical Fe₃O₄ NPs. Higher removal of Congo red dye from aqueous solution with higher adsorption capacity were achieved by the cubic of Fe₃O₄ NPs due to the magnetic properties. Finally, the equilibrium adsorption data of Congo red showed that cubic Fe₃O₄ NPs followed Langmuir isotherm model indicating a monolayer adsorption with a maximum adsorption capacity of 51.34 mg/g, while spherical Fe₃O₄ NPs followed Freundlich model, indicating a multilayer adsorption of Congo red.

ACKNOWLEDGEMENTS

This research was made possible by an NPRP Grant # 10-0127-170270 from the Qatar National Research Fund (a member of Qatar Foundation). The statements made herein are solely the responsibility of the authors. The Authors would like to also acknowledge the financial support of Universiti Kebangsaan Malaysia through DIP-2018-023 research grant.

FUNDING

Open Access funding provided by the Qatar National Library.

CONFLICT OF INTEREST

On behalf of all authors, the corresponding author states there is no conflict of interest.

OPEN ACCESS

This article is licensed under a Creative Commons Attribution 4.0 International License, which permits use, sharing, adaptation, distribution and reproduction in any medium or format, as long as you give appropriate credit to the original author(s) and the source, provide a link to the Creative Commons licence, and indicate if changes were made. The images or other third party material in this article are included in the article's Creative Commons licence, unless indicated otherwise in a credit line to the material. If material is not included in the article's Creative Commons licence and your intended use is not permitted by statutory regulation or exceeds the permitted use, you will need to obtain permission directly from the copyright holder. To view a copy of this licence, visit <http://creativecommons.org/licenses/by/4.0/>.

REFERENCES

1. S. Sadeghpour, A. Amirjani, M. Hafezi, and A. Zamanian, *Ceram. Int.* 40, 16107. (2014).
2. T. Zhao, J. Zai, M. Xu, Q. Zou, Y. Su, K. Wang, and X. Qian, *Cryst. Eng. Comm.* 13, 4010. (2011).
3. L. Qiao, Z. Fu, J. Li, J. Ghosen, M. Zeng, J. Stebbins, P. Prasad, and M. Swihart, *ACS Nano* 11, 6370. (2017).
4. S. Arteaga-Díaz, S. Meramo-Hurtado, J. León-Pulido, A. Zuorro, and A. González-Delgado, *Appl. Sci.* 9, 1682. (2019).
5. B. Richard, J. Lemyre, and A. Ritcey, *Langmuir* 33, 4748. (2017).
6. K. Hedayati, M. Goodarzi, and D. Ghanbari, *J. Nanostruct.* 7, 32. (2017).

7. D. Kim, N. Lee, M. Park, B.H. Kim, K. An, and T. Hyeon, *J. Am. Chem. Soc.* 131, 454. (2009).
8. D. Ghanbari and M. Salavati-Niasari, *Particuology*. 26, 87. (2016).
9. M. Kerroum, A. Essyed, C. Iacovita, W. Baaziz, D. Ihi-awakrim, O. Mounkachi, M. Hamedoun, A. Benyoussef, M. Benaissa, and O. Ersen, *J. Magn. Magn. Mater.* 478, 239. (2019).
10. R. Hachani, M. Lowdell, M. Birchall, A. Hervault, D. Mertz, S. Begin-Colin, and N.T.K. Thanh, *Nanoscale* 8, 3278. (2016).
11. A. Kostopoulou and A. Lappas, *J. Nanotechnol. Rev.* 4, 595. (2015).
12. J. Moradiganjeh and Z. Aghajani, *J. Mater. Sci.: Mater. Electron.* 27, 5948. (2016).
13. F. Ghasemy-Piranloo, S. Dadashian, and F. Bavarsiha, *J. Mater. Sci.: Mater. Electron.* 30, 12757. (2019).
14. Y. Yew, K. Shameli, S. Mohamad, Y. Nagao, S.-Y. Teow, K. Lee, and E. Isa, *Int. J. Pharm.* 572, 118743. (2019).
15. M. Ma, Y. Zhang, Z. Guo, and N. Gu, *Nanoscale Res. Lett.* 8, 16. (2013).
16. M. Dewi, W. Skinner, and T. Nann, *Aust. J. Chem.* 67, 663. (2014).
17. B. Lesiak, N. Rangam, P. Jiricek, I. Gordeev, J. Tóth, L. Kövér, M. Mohai, and P. Borowicz, *Front Chem.* 7, 642. (2019).
18. J.C. Rivière, *Surface analytical techniques* (Oxford Science Publications, Clarendon Press, Oxford, 1990).
19. A. Grosvenor, B. Kobe, and N. McIntyre, *Surf. Sci.* 565, 151. (2004).
20. N. Torres-Gómez, O. Nava, L. Argueta-Figueroa, R. García-Contreras, A. Baeza-Barrera, and A.R. Vilchis-Nestor, *J. Nanomater.* 2019, 7921273. (2019).
21. P. Coppola, F.G. da Silva, G. Gomide, F. Paula, A. Campos, R. Perzynski, C. Kern, J. Depeyrot, and R. Aquino, *J. Nanopart. Res.* 18, 138. (2016).
22. F. Ocan, *JOM* 73, 3702. (2021).
23. T.K. Sau and A.L. Rogach, *Adv. Mater.* 22, 1781. (2010).
24. A. Awad, R. Jalab, A. Benamor, M. Nasser, M. Ba-Abbad, and M. El-Naas, *J. Mol. Liq.* 301, 112335. (2020).
25. Z. Lou, Z. Zhou, W. Zhang, X. Zhang, X. Hu, P. Liu, and H. Zhang, *J. Taiwan. Inst. Chem. Eng.* 49, 199. (2015).
26. S. Chatterjee, N. Guha, S. Krishnan, A.K. Singh, P. Mathur, and D.K. Rai, *Sci. Rep.* 10, 111. (2020).
27. C. Ong, A. Mohammad, R. Rohani, M. Ba-Abbad, and N. Hairom, *Process Saf. Environ. Prot.* 104, 549. (2016).
28. L. Ai, C. Zhang, and Z. Chen, *Hazard. Mater.* 192, 1515. (2011).
29. M. Ba-Abbad, M. Takriff, A. Benamor, and A. Mohammad, *J. Sol-Gel Sci. Technol.* 81, 880. (2017).
30. A. Rostami-Vartooni, L. Rostami, and M. Bagherzadeh, *J. Mater. Sci.: Mater. Electron.* 30, 21377. (2019).
31. D. Ewis and B. Hameed, *J. Water Process Eng.* 41, 102006. (2021).
32. D. Ewis, A. Benamor, M. Ba-Abbad, M. Nasser, M. El-Naas, and H. Qiblawey, *J. Water. Process. Eng.* 38, 101583. (2020).

Publisher's Note Springer Nature remains neutral with regard to jurisdictional claims in published maps and institutional affiliations.